Journal of Sound and Vibration 442 (2019) 770–786

Contents lists available at ScienceDirect

Journal of Sound and Vibration

journal homepage: www.elsevier.com/locate/jsvi

Statistical quantification of DC power generated by bistable piezoelectric energy harvesters when driven by random excitations

Chunlin Zhang [a, b, *], Ryan L. Harne [c], Bing Li [d], K.W. Wang [b]

[a] School of Aeronautics, Northwestern Polytechnical University, Xi'an, Shaanxi, 710072, P.R. China
[b] Department of Mechanical Engineering, University of Michigan, Ann Arbor, MI 48105, USA
[c] Department of Mechanical and Aerospace Engineering, The Ohio State University, Columbus, OH 43210, USA
[d] State Key Laboratory for Manufacturing and Systems Engineering, Xi'an Jiaotong University, Xi'an, Shaanxi, 710049, PR China

ARTICLE INFO

Article history:
Received 1 August 2018
Received in revised form 31 October 2018
Accepted 19 November 2018
Available online 20 November 2018
Handling Editor: Ivana Kovacic

Keywords:
Bistable vibration energy harvesters
Standard rectifying electrical circuit
DC output power
White noise excitation
Stochastic averaging

ABSTRACT

Vibration energy harvesting provides prominent potential on leveraging the converted energy to realize self-powered electronics. To satisfy the demand of electronics and rechargeable batteries for DC voltages in practical applications, the high-performing, nonlinear bistable energy harvesters are considered to be interfaced with standard rectifying electrical circuits to extract DC power from environment-like, random base accelerations. To lead to an effective and efficient set of design guidelines for system development, this research proposes a theoretical method to characterize the stationary stochastic dynamic responses and the energy harvesting performance under white noise accelerations. Considering that the bistable harvesters possess multiple vibration regimes which induce drastically different energy harvesting performances, a novel state-probability estimation approach is presented based on the theoretically predicted probability density function (PDF) of system energy to statistically classify the stationary probability of the stochastic vibrations being in the snap-through or intrawell states. Via investigating the effects of the base acceleration strength and system parameters on the dynamic responses and harvested DC power, it is revealed that high energy harvesting performance would be achieved via low system damping and suitable system parameters, such as moderate coupling constant and load resistance. The theoretical predictions are compared with numerical simulations and experimental results to validate the effectiveness of the proposed theoretical method.

1. Introduction

Energy harvesting from environmental vibrations and human-induced motions has flourished as a prominent research area for running low-powered electronics and wireless sensor networks [1,2]. Nonlinear piezoelectric harvesters [3–6] especially bistable Duffing structures [7,8] possessing a double-well potential have drawn much attention due to the high-

* Corresponding author. School of Aeronautics, Northwestern Polytechnical University, Xi'an, Shaanxi, 710072, P.R. China.
E-mail address: zchunlin@nwpu.edu.cn (C. Zhang).

https://doi.org/10.1016/j.jsv.2018.11.032
0022-460X/

orbit well-escaping motion which is advantageous in both average harvested electric power and effective frequency bandwidth [9–11].

In order to improve the efficiency of piezoelectric energy harvesters and optimize the system parameters, it is important to quantify the harvestable electric power under vibration environments. To date, the system performances of bistable energy harvesters have been thoroughly studied using analytical [12,13], numerical [14,15], and experimental [16] techniques under various environmental excitations including harmonic [12,13,17], impulsive [18,19], and combined load [20] base accelerations. Collectively, these investigations demonstrated that snap-through oscillating from one stable equilibrium to another may be activated in a wide frequency bandwidth regardless of the input excitation forms, making bistable harvesters potentially more beneficial than alternative harvester platforms in various excitation environments.

Random noise is also a common environmental excitation since in many practical situations the ambient vibrations exhibit stochastic characteristics [21]. Stochastically excited bistable harvesters [22] have been extensively studied using a wide range of methods. For instance, Monte Carlo simulations [23–25], Finite Element analysis [21,26], and experimentally based approaches [27–29] have been employed to gain insight. Also, a theoretical technique based on the Fokker-Planck (FPK) equation directly derived from the nonlinear, second-order system governing equation is developed to analytically investigate the response probability density function, mean harvested powers, and effects of configuration, excitation intensity, and frequency bandwidth on the harvested electric power [30–32]. It is demonstrated that enhanced performance can be achieved by bistable harvesters instead of linear or monostable harvesters when appropriate potential energy function is designed to activate oscillations between the stable equilibria, and the optimal potential is related to the noise intensity under white noise excitations [27,33], while it is determined by the noise intensity and bandwidth under colored noise excitations [32,34]. These fruitful investigations exhibited the promising potential of bistable harvesters in engineering applications. On the other hand, in these studies the harvesting circuit connected with the piezoelectric element are simplified to be a resistive load (termed AC circuit for simplicity) [2,9,10], while most electronics and batteries in real applications require DC voltage. Thus, the electric circuit that interfaces the piezoelectric patch and terminal electronics must possess the capability to rectify the AC power to DC form, which is a highly nonlinear process.

In fact, several nonlinear electrical circuits have been investigated to obtain the DC power or enhance the energy conversion capability [35], including the standard rectifying circuit [36], synchronized switch harvesting on inductor (SSHI) [37] and the synchronous electric charge extraction (SECE) circuits [38]. Yet, such electric circuits are typically estimated when connected to a linear energy harvester, and their optimization strategies may no longer be ideal for nonlinear oscillations with multiple frequencies. To date, few attempts have been conducted to nonlinear, bistable harvesters interfaced with rectifying electrical circuits, among which the focus is primarily on harmonic-excitation situations [20,39–41]. There also remains a critical need for investigating the system when driven by environment-like, random base-acceleration excitations.

The goal of this research is to characterize the performance of randomly-excited bistable harvesters interfaced with the standard rectifying electrical circuit in which a full-wave diode bridge rectifier is adopted to convert the AC voltage to DC. Due to its advantages of passive operation manner, independency of external control and input energy, the standard rectifying electric circuit continues to draw much attention. For this kind of interfaced circuit, the diode-bridge alternatively conducts and blocks the current flowing into the rectifier capacitor according to the relative magnitude of the voltage across the piezoelectric patch and the rectified voltage across the load resistance, resulting to non-smooth, piecewise piezovoltage. Accordingly, the existing analytical method for investigating AC circuit interfaced bistable harvesters via solving the FPK equation of vibration variables [30–32] fails to directly analyze the standard rectifying electrical circuits interfaced bistable systems studied here. A theoretical method based on stochastic averaging method is proposed in this paper to provide a rigorous and systematic framework for predicting the joint and marginal probability density functions (PDFs) of vibration variables, and expectations of the rectified DC voltage and power. Through the validations of numerical simulation and experiments, the investigation also illustrates the effects of noise acceleration strength and system parameters on the system dynamics and energy harvesting performance.

The rest of this paper is organized as follows. The white noise excited bistable harvester interfaced with the standard rectifying circuit is modeled in Section 2. The mathematical formulas and procedures proposed to theoretically investigate the stationary performance under white noise acceleration are explained in Section 3. Section 4 illustrates the experimental system and corresponding system parameters which are used throughout in numerical and experimental efforts. In Section 5, both case examples and parameter studies are conducted to test the system performance in stationary state using the proposed theoretical method and numerical validations. Finally, the performance of the interfaced system with respect to noise acceleration strength is validated via experiments in Section 6.

2. System modeling

Most bistable energy harvesters in existing studies are implemented using buckled beam bridge [42], cantilevered ferromagnetic beam with repulsive [32] or attractive magnets [9], or bistable plates [10]. Despite the wide range of underlying principles to design these oscillators, it is well established that the lowest order dynamic behaviors can be described using the bistable Duffing equation [9]. In this study, a base-excited bistable oscillator having piezoelectric conversion mechanism is considered, in which the latter is further interfaced with a standard rectifying electrical circuit to convert the extracted AC voltage into DC form. Throughout this manuscript, the base acceleration excitation to which the bistable harvester is

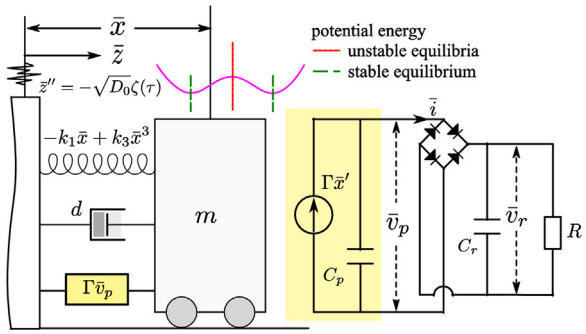

Fig. 1. Dynamic model of randomly-excited bistable harvester interfaced with a standard rectifying circuit.

subjected is assumed to be zero-mean Gaussian white noise. The system model is displayed in Fig. 1. The corresponding governing equations are expressed as

$$m\bar{x}'' + d\bar{x}' - k_1\bar{x} + k_3\bar{x}^3 + \Gamma\bar{v}_p = m\sqrt{D_0}\zeta(\tau) \tag{1a}$$

$$\Gamma\bar{x}' - C_p\bar{v}'_p = \bar{i} \tag{1b}$$

$$\bar{i} = \begin{cases} C_r\bar{v}'_r + \bar{v}_r/R, & \text{if } \bar{v}_p = \bar{v}_r \\ -C_r\bar{v}'_r - \bar{v}_r/R, & \text{if } \bar{v}_p = -\bar{v}_r \\ 0, & \text{if } |\bar{v}_p| < \bar{v}_r \end{cases} \tag{1c}$$

$$\langle\zeta(\tau_0), \zeta(\tau_1)\rangle = \delta(\tau_1 - \tau_0),\ E[\zeta(\tau)] = 0 \tag{1d}$$

in which, $\bar{x}$ denotes the relative displacement of mass m with respect to the base whose motion $\bar{z}$ is described using its acceleration as $\bar{z}'' = -\sqrt{D_0}\zeta(\tau)$ where the prime means the derivative with the time τ; $\sqrt{D_0}$ is the standard deviation of the Gaussian white noise, and reveals the strength of random accelerations; d, k_1 and k_3 represent the viscous damping constant, the linear, and nonlinear stiffness coefficients, respectively; Γ is the electromechanical coupling constant; the piezoelectric patch attached on the oscillator is equivalent to be current source of $\Gamma\bar{x}'$ in parallel with the capacitance C_p across which the transformed voltage is $\bar{v}_p$; $\bar{i}$ denotes the current flow through the diode bridge which rectifies the piezovoltage $\bar{v}_p$ into DC form across the filter capacitance C_r in parallel with the load resistance R; $\langle\zeta(\tau_0), \zeta(\tau_1)\rangle$ is the inner product of $\zeta(\tau_0)$ and $\zeta(\tau_1)$; $E[\zeta]$ is the expectation of ζ; and $\delta(\tau)$ is the Dirac delta function. In industry applications, relatively large C_r is generally adopted such that to provide near-constant rectified voltage $\bar{v}_r$ for electronics and rechargeable batteries. The structure may exhibit high-orbit snap-through vibrations around three equilibrium points including two stable equilibria $\bar{x}^* = \pm\sqrt{k_1/k_3}$ m and one unstable equilibrium $\bar{x}^* = 0$, or low-orbit intrawell vibrations that oscillate around one of the stable equilibria. Although the harvester oscillates between snap-through and intrawell regimes at random when under white noise excitations, the statistics are stationary and could be estimated to describe the transient dynamics properties.

In the analysis hereafter, a new time scale is adopted as $t = \omega_n\tau$, in which $\omega_n = \sqrt{k_1/m}$ represents the linear natural frequency of the mechanical oscillator. Introduce the following new non-dimensional parameters:

$$x_0 = \sqrt{k_1/k_3},\ x = \bar{x}/x_0,\ \gamma = d/m\omega_n,\ \beta = k_3x_0^2\big/k_1 \equiv 1,\ \Theta = \Gamma^2\big/m\omega_n^2C_p,\ v_p = C_p\bar{v}_p/\Gamma x_0 \tag{2a}$$

$$v_r = C_p\bar{v}_r/\Gamma x_0,\ \lambda = 1/RC_p\omega_n,\ \eta = C_r/C_p,\ i = \bar{i}\big/\Gamma\omega_n x_0,\ \sqrt{2D} = \sqrt{D_0}\big/\omega_n^2x_0 \tag{2b}$$

The non-dimensional governing equations are thus derived to be:

$$\ddot{x} + \gamma\dot{x} - x + \beta x^3 + \Theta v_p = \sqrt{2D}\cdot\zeta(t) \tag{3a}$$

$$\dot{x} - \dot{v}_p = i \tag{3b}$$

$$i = \begin{cases} \eta\dot{v}_r + \lambda v_r, & \text{if } v_p = v_r \\ -\eta\dot{v}_r - \lambda v_r, & \text{if } v_p = -v_r \\ 0, & \text{if } |v_p| < v_r \end{cases} \tag{3c}$$

$$\langle \zeta(t_0), \zeta(t_1) \rangle = \delta(t_0 - t_1),\ E[\zeta(t)] = 0 \tag{3d}$$

in which the over-dot operator means the derivative of the variables with the time t. Considering $\zeta(t)$ is resampled series of the uniform white noise $\zeta(\tau)$ with the linear scale of $t = \omega_n \tau$, the standard deviation of $\zeta(t)$ will be the same with that of $\zeta(\tau)$. It is noted that the stable and unstable equilibria of the equivalent non-dimensional system are respectively $x^* = \pm\sqrt{1/\beta} = \pm 1$, and $x^* = 0$.

3. Dynamics quantification using stochastic averaging method of energy envelope

The converted piezovoltage exhibits piecewise property due to the alternative block and conduct of the diode bridge in the standard rectifying electrical circuits. Thus, the existing analytical method for investigating AC circuit interfaced bistable harvesters via solving the FPK equation of vibration variables, as well as the standard stochastic averaging method, fails to directly analyze the standard rectifying electrical circuits interfaced bistable systems studied here. To investigate the system performance governed by Eq. (3), an improved theoretical method is proposed in this work. Considering most vibration energy harvesters are designed to be underdamped with a small damping coefficient γ, and the excitation acceleration intensity $\sqrt{2D}$ in the non-dimensional equations is small due to the large scaling factor $\omega_n^2 x_0$ in Eq. (2b), thus Eq. (3) represents a quasi-conservative system, i.e., the difference between the input energy due to external acceleration excitation and the energy dissipated by damping is relatively smaller than the total energy, and thus permits the theoretical investigation via stochastic averaging approach [43]. In the stochastic averaging analysis, the total energy is also termed as energy envelope of the system which consists of kinetic and potential energies of the harvester [44].

According to the generalized harmonic transformation technique [45], the non-dimensional, equivalent displacement and velocity can be expressed as:

$$x = A(H)\cdot\cos(\omega(H)t) + c(H) \tag{4a}$$

$$\dot{x} = -A(H)\omega(H)\cdot\sin(\omega(H)t) \tag{4b}$$

where $H \equiv H(t)$ is the total energy, and is regarded as slow-varying for stationary responses in comparison with the rapidly-varying displacement and velocity; $A(H)$ and $\omega(H)$ represent the energy-dependent vibration amplitude and frequency, respectively; $c \equiv c(H)$ denotes the displacement offset of the bistable oscillator, and thus satisfies $c = 0$ for large-orbit snap-through oscillations. From Eq. (4), the displacement and velocity could be approximated as a periodic oscillation with a pseudo period $T = 2\pi/\omega(H)$.

3.1. Transduced piezovoltage coupling relation to the dynamic responses

To meet the requirement of DC voltage for most electronics, a relatively large filter capacitance C_r is applied such that the rectified voltage v_r could be assumed near-constant. The diode bridge in the standard rectifying electrical circuit alternatively conducts and blocks; i.e., the bridge conducts and $i \neq 0$ when the absolute value of the piezovoltage reaches the rectified voltage $|v_p| = v_r$, while it blocks during the period when $|v_p| < v_r$, resulting in piecewise piezovoltage v_p. Assuming the diode is ideal, such that there is no voltage-drop when the current flows through, v_p could be mathematically derived from Eqs. (3b) and (3c), and the displacement and velocity in Eq (4).

$$v_p = \begin{cases} A(\cos\omega t - 1) + v_r, & \omega t \in [0, \theta) \\ -v_r, & \omega t \in [\theta, \pi) \\ A(\cos\omega t + 1) - v_r, & \omega t \in [\pi, \pi + \theta) \\ v_r, & \omega t \in [\pi + \theta, 2\pi] \end{cases} \tag{5}$$

where θ is the rectifier blocked angle in half an equivalent oscillation cycle, and satisfies

$$A(\cos\theta - 1) + v_r = -v_r \tag{6}$$

Considering that the total charge flows into the electrical circuit equals that consumed by the resistive load during half the equivalent motion cycle in stationary, as well as the rectified voltage is nearly constant, the integration of Eq. (3b) on the interval of $0 \le \omega t \le \pi$ equals that of Eq. (3c).

$$\int_0^{\pi}(\dot{x}-\dot{v}_p)\mathrm{d}\omega t=-2A+2v_r=\int_0^{\pi}(-\eta\dot{v}_r-\lambda v_r)\mathrm{d}\omega t\approx-\lambda v_r\pi/\omega \tag{7}$$

From Eqs. (6) and (7), v_r and θ can be solved and expressed as:

$$v_r=\frac{2A}{2+\lambda\pi/\omega} \tag{8}$$

$$\cos\theta=1-\frac{4}{2+\lambda\pi/\omega} \tag{9}$$

Adopting the strategy in previous research of harmonically-excited case [46], the piecewise piezovoltage is further represented using its smooth, fundamental harmonic component.

$$v_{p,f}=\frac{A}{2\pi}(2\theta-\sin 2\theta)\cos\omega t-\frac{A}{\pi}\sin^2\theta\sin\omega t=\frac{1}{2\pi}(2\theta-\sin 2\theta)\cdot(x-c)+\frac{\sin^2\theta}{\pi\omega}\dot{x} \tag{10}$$

Submitting Eq. (10) into (3a), the equivalent dynamic equation is derived to be

$$\ddot{x}+(\gamma+J_H)\dot{x}+(N_H-1)x+\beta x^3-N_H\cdot c=\sqrt{2D}\cdot\zeta(t) \tag{11a}$$

$$J_H=\frac{\Theta}{\pi\omega}\sin^2\theta,\quad N_H=\frac{\Theta}{2\pi}\cdot(2\theta-\sin 2\theta) \tag{11b}$$

Here, both J_H and N_H are functions of the total energy. The advantage of this strategy is approximating the piecewise dynamics with a smooth, equivalent dynamic system from the power point of view.

3.2. Relation estimation of vibration variables to the total energy

Similar with the total energy, the equivalent vibration amplitude and frequency are also slow-varying, and are thus regarded as constant while the displacement x varies through a pseudo period. Moreover, the equivalent vibration amplitude and frequency are system energy dependent, and their relations are investigated in this section.

3.2.1. Equivalent vibration amplitude

Recalling Eq. (11), the potential energy of the bistable harvester is calculated as:

$$V_p(x,H)=\frac{N_H-1}{2}x^2+\frac{\beta}{4}x^4+\Delta=\frac{\beta}{4}\left(x^2-\frac{1-N_H}{\beta}\right)^2-\frac{(1-N_H)^2}{4\beta}+\Delta \tag{12}$$

where $\Delta=(1-N_H)^2/4\beta$, such that the minimum point of the potential energy is set at 0. The barrier height is thus $V_p(0,H)=(1-N_H)^2/4\beta$. Accordingly, the total energy is obtained when the kinetic and potential energies are taken into account:

$$H=\frac{1}{2}\dot{x}^2+V_p(x,H)=\frac{1}{2}\dot{x}^2+\frac{\beta}{4}\left(x^2-\frac{1-N_H}{\beta}\right)^2 \tag{13}$$

The bistable harvester possesses two different kinds of oscillations: large-orbit snap-through vibration spanning between two potential wells, and low-orbit intrawell vibration limited in only one potential well. Thus, for this quasi-conservative system, the harvester performs intrawell oscillations when the system energy meets $0<H\le(1-N_H)^2/4\beta$; while undergoes snap-through vibrations when the system energy overreaches the barrier height $H\ge(1-N_H)^2/4\beta$. The energy separatrix $H=(1-N_H)^2/4\beta$ corresponds to the homoclinic orbit on which the vibration period trends to be infinite.

Considering the total energy equals the potential energy at the extremal points of the displacement where the velocity is 0, one obtains

$$H=V_p(x_{c,d},H)=\frac{N_H-1}{2}x_{c,d}^2+\frac{\beta}{4}x_{c,d}^4+\frac{(1-N_H)^2}{4\beta} \tag{14}$$

where the subscript c and d indicates the dynamic behaviors of the displacement in the snap-through and intrawell regimes, respectively. For intrawell vibrations, considering that the four roots of Eq. (14) are distributed symmetrically on both sides of the unstable equilibrium $x^*=0$, only the displacement range on the positive axis is considered here. The minimum x_{d1} and maximum x_{d2} of the displacement for intrawell vibration can thus be obtained

$$x_{d1} = \left[(1 - N_H)/\beta - \sqrt{4H/\beta}\right]^{1/2} \tag{15a}$$

$$x_{d2} = \left[(1 - N_H)/\beta + \sqrt{4H/\beta}\right]^{1/2} \tag{15b}$$

The equivalent vibration amplitude of intrawell oscillations can thus be estimated to be:

$$A_d(H) = (x_{d2} - x_{d1})/2 = \left\{\left[(1 - N_H)/\beta + \sqrt{4H/\beta}\right]^{1/2} - \left[(1 - N_H)/\beta - \sqrt{4H/\beta}\right]^{1/2}\right\}\Big/2 \tag{16}$$

On the other hand, for snap-through oscillations span between the two potential wells, Eq. (14) possesses two real roots, indicating the boundaries of the displacement.

$$x_{c1} = -\left[(1 - N_H)/\beta + \sqrt{4H/\beta}\right]^{1/2} \tag{17a}$$

$$x_{c2} = \left[(1 - N_H)/\beta + \sqrt{4H/\beta}\right]^{1/2} \tag{17b}$$

where x_{c1} and x_{c2} indicate the minimal and maximal points of the displacement, respectively. And the vibration amplitude of snap-through oscillations can thus be obtained.

$$A_c(H) = (x_{c2} - x_{c1})/2 = \left[(1 - N_H)/\beta + \sqrt{4H/\beta}\right]^{1/2} \tag{18}$$

3.2.2. Equivalent vibration frequency

From Eq. (13), the velocity under given system energy is derived to be

$$\dot{x} \equiv \mathrm{d}x/\mathrm{d}t = \sqrt{2(H - V_p(x,H))} \tag{19}$$

Considering the harvester oscillates in the range of $[x_{d1}, x_{d2}]$ for intrawell vibrations and $[x_{c1}, x_{c2}]$ for snap-through vibrations, the pseudo period of the vibration $T(H)$ can be estimated using

$$T_{d(c)}(H) = 2\int_{x_{d1(c1)}}^{x_{d2(c2)}} 1\Big/\sqrt{2(H - V_p(x,H))}\,\mathrm{d}t \tag{20}$$

Combining Eqs. (13) and (14), the kinetic energy of the harvester, $H - V_p$, is further derived and expressed as:

$$H - V_p = V_p(x_{c,d}, H) - V_p(x,H) = \frac{\beta}{4}\left(x_{d2(c2)}^2 - x^2\right)\left(x^2 - x_{d1(c1)}^2\right) \tag{21}$$

Submitting Eq. (21) into (20), the pseudo vibration period for intrawell vibrations can be derived and simplified.

$$T_d(H) = 2\int_{x_{d1}}^{x_{d2}} \frac{\sqrt{2}}{\sqrt{\beta}} \cdot \frac{1}{\sqrt{\left(x_{d2}^2 - x^2\right)\left(x^2 - x_{d1}^2\right)}}\,\mathrm{d}x = \frac{2\sqrt{2}}{\sqrt{\beta}} \cdot g_d \cdot K(\vartheta_d) \tag{22}$$

where $K(\cdot)$ is the complete elliptic integral of the first kind [47]; g_d and ϑ_d can be expressed as:

$$g_d = \sqrt{\beta}\Big/\sqrt{1 - N_H + \sqrt{4H\beta}}, \vartheta_d = 2\left[\sqrt{H\beta}\Big/\sqrt{1 - N_H + \sqrt{4H\beta}}\right]^{1/2} \tag{23}$$

On the other hand, for the snap-through vibration regime, the pseudo period is obtained from Eq. (20).

$$T_c(H) = 4\int_0^{x_{c2}} \frac{\sqrt{2}}{\sqrt{\beta}} \cdot \frac{1}{\sqrt{(x_{c2}^2 - x^2)(x^2 - x_{c1}^2)}} \cdot \mathrm{d}x = \frac{4}{\sqrt{\beta}} \cdot g_c \cdot K(\vartheta_c) \tag{24}$$

where the parameters g_c and ϑ_c can be expressed as:

$$g_c = (4H/\beta)^{-1/4},\ \vartheta_c = \left[\left(1 - N_H + 2\sqrt{H\beta}\right) \Big/ \sqrt{H\beta}\right]^{1/2} \Big/ 2 \tag{25}$$

Noting that the pseudo vibration period also meets $T_{d(c)}(H) = 2\pi/\omega_{d(c)}(H)$, for vibrations in the intrawell regime, the vibration frequency $\omega_d(H)$ satisfies

$$2\sqrt{2} \Big/ \sqrt{1 - N_H + 2\sqrt{H\beta}} \cdot K\left[2(\sqrt{H\beta}/\sqrt{1 - N_H + 2\sqrt{H\beta}}\,)^{1/2}\right] = 2\pi/\omega_d \tag{26}$$

While for vibrations in the snap-through regime, the vibration frequency $\omega_c(H)$ satisfies

$$4 \Big/ \sqrt{\beta} \cdot (4H/\beta)^{-1/4} \cdot K\left[(1 - N_H + 2\sqrt{H\beta}/\sqrt{H\beta}\,)^{1/2} \Big/ 2\right] = 2\pi/\omega_c \tag{27}$$

Thus, the equivalent vibration frequencies of the intrawell and snap-through vibrations can be solved via solving the roots of Eqs. (26) and (27), respectively. For given total energy H, recalling N_H is the function of $\omega(H)$ based on Eqs. (9) and (11b), Eqs. (26) and (27) are thus equations with one unknown variable of $\omega(H)$. The Eqs. (26) and (27) may therefore be solved via root finding algorithms such as the *fsolve* command in the MATLAB software used for this research.

3.3. Stochastic averaging method of energy envelope

Introducing $X_1 = x$ and $X_2 = \dot{x}$, the Itô stochastic differential equations associated with the equivalent nonlinear system in Eq. (11) can be directly derived.

$$\mathrm{d}X_1 = X_2 \mathrm{d}t \tag{28a}$$

$$\mathrm{d}X_2 = \left[-(\gamma + J_H)X_2 - (N_H - 1)X_1 - \beta X_1^3 + N_H \cdot c\right]\mathrm{d}t + \sqrt{2D} \cdot \mathrm{d}B(t) \tag{28b}$$

in which, $B(t)$ is a unit Weiner process. Considering the variable relations of $\dot{X}_1 = X_2$ and $H = X_2^2/2 + V_p(X_1, H)$, the above Itô equations for system displacement and velocity can thus be transformed into the following Itô equations with respect to the total energy [48].

$$\mathrm{d}X_1 = \pm\sqrt{2H - 2V_p}\mathrm{d}t \tag{29a}$$

$$\mathrm{d}H = \left\{\left[\frac{\partial H}{\partial X_1} \quad \frac{\partial H}{\partial X_2}\right]\begin{bmatrix} X_2 \\ -(\gamma + J_H)X_2 - (N_H - 1)X_1 - \beta X_1^3 + N_H \cdot c \end{bmatrix} + D \cdot \frac{\partial^2 H}{\partial X_2^2}\right\}\mathrm{d}t + \sqrt{2D} \cdot \frac{\partial H}{\partial X_2} \cdot \mathrm{d}B(t) \tag{29b}$$

In Eq. (29), the partial derivatives of system energy H to the displacement X_1 and velocity X_2 can be calculated using the following formula:

$$\frac{\partial H}{\partial X_1} = \frac{\partial V_p(X_1, H)}{\partial H} \cdot \frac{\partial H}{\partial X_1} + \frac{\partial V_p(X_1, H)}{\partial X_1} \ \Rightarrow\ \frac{\partial H}{\partial X_1} = \frac{\partial V_p(X_1, H)/\partial X_1}{1 - \partial V_p(X_1, H)/\partial H} \tag{30a}$$

$$\frac{\partial H}{\partial X_2} = X_2 + \frac{\partial V_p(X_1, H)}{\partial H} \cdot \frac{\partial H}{\partial X_2} \ \Rightarrow\ \frac{\partial H}{\partial X_2} = \frac{X_2}{1 - \partial V_p(X_1, H)/\partial H} \tag{30b}$$

$$\frac{\partial^2 H}{\partial X_2^2} = \frac{1}{1 - \partial V_p(X_1, H)/\partial H} + \frac{X_2^2 \cdot \partial^2 V_p(X_1, H) \Big/ \partial H^2}{\left(1 - \partial V_p(X_1, H)/\partial H\right)^3} \tag{30c}$$

It is seen that the right side of Eq. (29) are functions of the displacement and system energy. For the quasi-conservative system with underlying relatively small damping constant and external excitation acceleration density, the energy-envelope process H, is slow-varying compared with the rapidly-varying displacement, and could be regarded as near-constant through a pseudo period. Based on the Khasminskii theory, the H process converges weakly to a one-dimensional Markov process [49]. The Itô equation for this Markov process is further obtained via applying time averaging operation to Eq. (29b). With the

assistance of Eq. (29a), the time averaging operation can be transferred to averaging with respect to the displacement X_1, under the assumption that the total energy keeps near constant during a pseudo vibration period of the displacement. The resulting Itô equation is given by

$$\mathrm{d}H = U(H)\mathrm{d}t + \sigma(H)\mathrm{d}B(t) \tag{31}$$

where the drift coefficient $U(H)$ and diffusion coefficient $\sigma(H)$ are piecewise functions consisting of separated expressions for the intrawell and snap-through regimes. The subscript d denotes the intrawell vibration regime in the range of $0 < H \le (1-N_H)^2/4\beta$, while c corresponds to the snap-through regime in the range of $H \ge (1-N_H)^2/4\beta$.

$$U_{d(c)}(H) = \frac{2}{T_{d(c)}(H)}\left\{\int_{x_{d1(c1)}}^{x_{d2(c2)}} -\frac{\gamma + J_H}{1-\partial V_p/\partial H}\cdot\sqrt{2H-2V_p}\,\mathrm{d}X_1 + \int_{x_{d1(c1)}}^{x_{d2(c2)}}\frac{N_H\cdot c}{1-\partial V_p/\partial H}\mathrm{d}X_1\right\} + \frac{2}{T_{d(c)}(H)}\left\{\int_{x_{d1(c1)}}^{x_{d2(c2)}}\frac{D}{(1-\partial V_p/\partial H)\sqrt{2H-2V_p}}\mathrm{d}X_1 + \int_{x_{d1(c1)}}^{x_{d2(c2)}}\frac{D\sqrt{2H-2V_p}\cdot\partial^2 V_p/\partial H^2}{(1-\partial V_p/\partial H)^3}\mathrm{d}X_1\right\} \tag{32a}$$

$$\sigma_{d(c)}^2(H) = \frac{4D}{T_{d(c)}(H)}\cdot\int_{x_{d1(c1)}}^{x_{d2(c2)}}\frac{\sqrt{2H-2V_p}}{(1-\partial V_p/\partial H)^2}\mathrm{d}X_1 \tag{32b}$$

$$T_{d(c)}(H) = 2\pi\Big/\omega_{d(c)}(H) \tag{32c}$$

The Fokker-Planck equation corresponding to the Itô equation (31) is

$$\frac{\partial p(H)}{\partial t} = -\frac{\partial[U(H)p(H)]}{\partial H} + \frac{1}{2}\cdot\frac{\partial^2[\sigma^2(H)p(H)]}{\partial H^2} \tag{33}$$

where $p(H)$ is the probability density function of the system energy H, and its boundary condition at $H=0$ is finite while satisfies

$$p(H),\ \ \partial p(H)/\partial H|_{H\to\infty} \to 0 \tag{34}$$

The stationary solution of Eq. (33) can be obtained analytically based on $\partial p(H)/\partial t = 0$.

$$p(H) = \frac{C}{\sigma^2(H)}\cdot\exp\left[\int_0^H\frac{2U(y)}{\sigma^2(y)}\mathrm{d}y\right] \tag{35}$$

where C is the normalization constant and expressed to be

$$C = 1\Big/\int_0^\infty\exp\left[\int_0^H 2U(y)\Big/\sigma^2(y)\mathrm{d}y\right]\Big/\sigma^2(H)\mathrm{d}H \tag{36}$$

3.4. Electric power and stationary PDF estimation

Combining Eqs. (8) and (35), the expectation of the rectified voltage across the load resistance is predicted via integration based on the probability density function $p(H)$.

$$E(v_r) = \int_0^{(1-N_H)^2/4\beta}\frac{2A_d(H)}{2+\lambda\pi/\omega_d(H)}\cdot p(H)\mathrm{d}H + \int_{(1-N_H)^2/4\beta}^\infty\frac{2A_c(H)}{2+\lambda\pi/\omega_c(H)}\cdot p(H)\mathrm{d}H \tag{37}$$

Based on the assumption that the rectified voltage keeps near constant when relatively large filter capacitance is adopted, the expectation of non-dimensional, harvested electric power is:

$$E(P_r) = E\left[\frac{v_r^2}{1/\lambda}\right] = \lambda\cdot[E(v_r)]^2 \tag{38}$$

Recalling that the real, harvested electric power of the system in Eq. (1) meets $\overline{P}_r = \overline{v}_r^2/R$, the relation of the real and non-dimensional electric powers is thus given by $\overline{P}_r = P_r \cdot I^2 x_0 \omega_n / C_p$. Considering that the intrawell and snap-through vibration regimes correspond to different system energy ranges [50], the accumulative probability of $p(H)$ in the energy range of $0 < H \leq (1-N_H)^2/4\beta$ and $H \geq (1-N_H)^2/4\beta$, termed F_d and F_c, can thus be defined as state probability indicators to classify the stationary probability of the stochastic vibrations being in the snap-through or intrawell states.

$$F_d = F|_{0<H\leq(1-N_H)^2/4\beta} = \int_0^{(1-N_H)^2/4\beta} p(H)\mathrm{d}H \tag{39}$$

$$F_c = F|_{H\geq(1-N_H)^2/4\beta} = \int_{(1-N_H)^2/4\beta}^{\infty} p(H)\mathrm{d}H \tag{40}$$

Moreover, based on the stationary probability density function of the system energy, the stationary joint probability density function of displacement x and velocity $\dot{x}$ can be evaluated. In the intrawell vibration regime with the system energy satisfying $0 < H \leq (1-N_H)^2/4\beta$, the transformation from $p(H)$ to $p(x,\dot{x})$ is one-to-two mapping for each H level based on the theory of Stratonovitch [51]. Recalling that the two potential wells of the bistable harvester considered here are strictly symmetric, the probability density in each well is thus assumed to be the same. This yields to the following approximate joint probability density function for the displacement and velocity in the intrawell vibration regime.

$$p(x,\dot{x}) = \frac{1}{2}\cdot\frac{p(H)}{T_d(H)}\bigg|_{H(x,\dot{x})} = \left.\frac{\frac{p(H)}{2}}{\frac{2\sqrt{2}}{\sqrt{1-N_H+2\sqrt{H\beta}}}\cdot K\left[2\left(\frac{\sqrt{H\beta}}{1-N_H+2\sqrt{H\beta}}\right)^{1/2}\right]}\right|_{H=\frac{x^2}{2}+\frac{\beta\left(x^2-\frac{1-N_H}{\beta}\right)^2}{4},\ 0<H\leq\frac{(1-N_H)^2}{4\beta}} \tag{41}$$

On the other hand, in the snap-through vibration regime with the system energy $H \geq (1-N_H)^2/4\beta$, the transformation from $p(H)$ to $p(x,\dot{x})$ is one-to-one mapping for each H level and the joint probability density can thus be given as:

$$p(x,\dot{x}) = \frac{p(H)}{T_c(H)}\bigg|_{H(x,\dot{x})} = \left.\frac{p(H)}{\frac{4}{\sqrt{\beta}}\cdot\left(\frac{4H}{\beta}\right)^{-1/4}\cdot K\left[\left(\frac{1-N_H+2\sqrt{H\beta}}{4\sqrt{H\beta}}\right)^{1/2}\right]}\right|_{H=\frac{x^2}{2}+\frac{\beta\left(x^2-\frac{1-N_H}{\beta}\right)^2}{4},\ H\geq\frac{(1-N_H)^2}{4\beta}} \tag{42}$$

Accordingly, the marginal probability density functions $p(x)$ and $p(\dot{x})$ can be obtained as follows:

$$p(x) = \int_{-\infty}^{+\infty} p(x,\dot{x})\mathrm{d}\dot{x} \tag{43a}$$

$$p(\dot{x}) = \int_{-\infty}^{+\infty} p(x,\dot{x})\mathrm{d}x \tag{43b}$$

4. Experimental setup and system parameters

The system parameters utilized throughout the following analytical and numerical studies correspond to the experimental system explored in this research. A piezoelectric cantilever with ferromagnetic beam substrate is used where the substrate has length 135.83mm, width 12.70mm and thickness 0.51mm. Two attractive magnets spaced symmetrically around both sides of the cantilever tip with their center-to-center distance of 23.81mm. As shown in Fig. 2, the steel beam was cantilevered horizontally to eliminate the gravitational influence on dynamic responses, and the primary generalized displacement is thus the beam tip motion. The combination of the elastic and magnetic restoring forces exerts the beam tip, inducing the bistability of the ferromagnetic beam. A piezoelectric patch of length 25.40mm and width 12.70mm was bonded to the beam surface using silver epoxy (MG Chemicals 8831) with the patch center spaced from the cantilevered end by 32.00mm. The two piezoelectric electrodes were then interfaced with a standard diode bridge-based rectifying electrical circuit in which the filter capacitance and load resistance are adopted as 47μF and 100kΩ, respectively. Via adjusting the two magnets, the stable equilibria of the beam tip are measured at $x^* = \pm 6.6$mm and the two intrawell natural frequencies are measured to be 27.64Hz and 27.15Hz, indicating that the configuration possesses close to ideally symmetric double-well potential. The mechanical bistable oscillator was mounted on an electrodynamic shaker (APS ELECTRO-SEIS) of which the motion can be exactly controlled by the National Instruments output channel through a LABVIEW software interface, as well as the input

gain of the shaker. An accelerometer (PCB-352C33) is fixed at the end of the shaker to track the base acceleration. A laser interferometer (Polytec OFV-3001, OFV-5000) is used to measure the vibration displacement and velocity of the bistable beam at the point which was attached with a reflector and 39.69mm away from the free end of the beam. Measurements of the rectified voltage across the load resistance and voltage drop through a diode were also acquired via the National Instruments input channel.

To identify the system parameters, the free vibrations of the bistable beam were recorded when the piezoelectric electrodes were interfaced directly with the load resistance R [18]. The relevant system parameters corresponding to the governing Eq. (1) were thus identified from measurements (e.g., the damping constant by the log-decrement method, or capacitance by multi-meter readout) or effective relations (e.g., the equivalent mass of a cantilevered beam from Ref. [52]) and presented in Table 1. According to the non-dimension transformation relation in Eq. (2), the non-dimensional system parameters are thus calculated and listed in Table 2.

5. Numerical validation of the theoretical formulation

In this section, the system performances in stationary vibrations are statistically quantified using the theoretical formulas under different noise acceleration densities, and the influences of system parameters on harvested electric powers are also studied. To test the fidelity of the theoretical method developed, the theoretical predictions are compared with the direct numerical simulation of the governing Eq. (3) using Milstein method under Gaussian white noise excitations [53]. In the numerical integration of Eq. (3), an integration step-size of $h = 0.001$ is set for Milstein calculations to ensure a high exactness of the simulations, and a long time-interval dynamic responses with more than 10^8 time samples are evaluated for estimation of the PDFs of variables as well as the expectations of rectified voltage and harvested electric power.

5.1. Case study: PDFs of vibration variables, and harvested electric power

Two representative cases in which the dominant oscillating state of the bistable harvester is separately in the intrawell and snap-through regimes are studied here to test the performance of the theoretical method on predicting the PDFs of the variables. Fig. 3 shows the results from relatively weak random acceleration excitation with the intensity $\sqrt{2D} = 3.162 \times 10^{-2}$, in which (a, b) are respectively the PDF of system energy, and joint PDF of the displacement and velocity; (c, d) display the marginal probability density of the displacement and that of the velocity, respectively. The solid curves in Fig. 3(a, c, and d) denote the theoretical predictions, while the circles correspond to the numerical counterparts evaluated using the *ksdensity* command in the MATLAB software. It is noted that the instantaneous system energy series for numerically evaluating its PDF in Fig. 3(c) are calculated from Eq. (13) based on simulated displacements and velocities with the assumption that $N_H = 0$, which exists for weak electromechanical coupling cases, and the numerical joint PDF in Fig. 3(b) are estimated in the MATLAB software using the *kde2d* function developed by Botev [54].

Apparently, the notable $p(H)$ locates in the range $H < \Delta$ with the theoretical prediction $F_c = 0$ in Fig. 3(a), indicating that the adopted weak excitation acceleration strength is insufficient for overcoming the potential barrier of the bistable harvester. That is unanimous with the symmetrically distributed $p(x, \dot{x})$ around the two stable equilibria in Fig. 3(b), as well as the

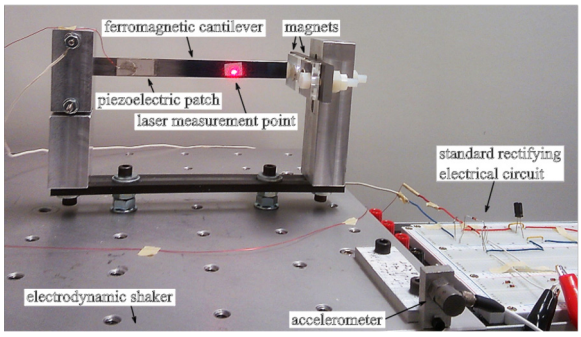

Fig. 2. Experimental system of a piezoelectric, bistable cantilever interfaced with a standard rectifying electrical circuit.

Table 1
Parameters of the experimental setup.

mass, m [g]	damping, d [N•s/m]	stiffness, k_1 [N/m]	stiffness, k_3 [N/m^3]
1.6	6.97×10^{-3}	23.59	5.46×10^{5}
coupling, Γ [N/V]	piezo capacitance, C_p[F]	filter capacitance, C_r[F]	resistance, R [kΩ]
0.081×10^{-3}	1.27×10^{-8}	4.7×10^{-5}	100

Table 2
Non-dimensional system parameters used throughout following analysis and numerical simulations.

parameter	γ	β	Θ	η	λ
value	0.0359	1	0.0219	3.7008×10^{3}	6.4688

notable $p(x)$ limited in the local potential wells shown in Fig. 3(c). Comparing with numerical PDFs, it is concluded that the theoretical predictions are basically in very good agreement with simulation results. And the theoretically predicted harvested voltage $E(v_r) = 0.01444$ is as close to that from numerical simulation with mean value $E(v_r) = 0.01276$ and standard deviation $\sigma_{v_r} = 0.001657$. Additionally, deviation between theoretical and numerical PDFs is captured in Fig. 3(a) on $p(H)$ near at $H = 0$ corresponding to the stationary vibration state of the harvester. The deviation results from the period averaging operation in the theoretical method which locally smooths the dramatically increased, impulse-like PDF of the system energy at $H = 0$ (as the circles shown in Fig. 3(a)).

Considering that $H = 0$ corresponds to the stationary vibration state where the harvester stays at stable equilibria with null velocity $\dot{x}\equiv0$, the local inaccuracy of the theoretically predicted $p(H = 0)$ further affects the predictions of the variable PDFs at a few localized positions, including $p(x)$ at the stable equilibria, and $p(\dot{x})$ at $\dot{x} = 0$, and $p(x,\dot{x})$ around the state ($x = 0$, $\dot{x} = 0$), as shown in the insets of Fig. 3(c), (d) and (b), respectively. Conclusively, the averaging operation sacrifices the prediction accuracy of $p(H)$ at a very few locations, but leads to solvable and explicit expression of $p(H)$.

Fig. 4 shows the theoretical predictions with numerical simulation results of the harvester system driven by relatively larger random acceleration with the intensity $\sqrt{2D} = 2.6886\times10^{-1}$. Different from the case in Fig. 3, the notable $p(H)$ in Fig. 4(a) mainly locates in the range $H>\Delta$ according to the logarithmic changes of the system energy, indicating that the dominant oscillating states of the harvester are in the snap-through regime which is theoretically predicted to be $F_c = 73.30\%$ and evidenced by the apparently distributed trajectories of $p(x,\dot{x})$ outside the homoclinic orbit in Fig. 4(b), as well as the notable $p(x)$ span the two stable equilibria in Fig. 4(c). Considering the PDFs of the vibration variables, it is apparent that the theoretical predictions correctly track the numerical results excepting at special locations as illustrated in the insets in Fig. 4(b)–(d) due to the weakness of the theoretical method in predicting the $p(H)$ at $H = 0$. Additionally, a singular jump is presented in Fig. 4(a) on the theoretically predicted $p(H)$ at $H = \Delta$ which corresponds to the homoclinic orbit. This undesirable deviation on the theoretical prediction is induced because the vibration state at $H = \Delta$ owning infinite vibration period doesn't satisfy the presupposition of the stochastic averaging operation which requires the averaged variables are near constant during the oscillation period. Through the tradeoff of the theoretical approach in predicting $p(H)$ in two extremal points of $H = 0$ and $H = \Delta$, this studied case reveals that the theoretical method provides a good approximation of the harvested rectified voltage in consideration of the predicted voltage $E(v_r) = 0.11266$ when compared with the simulated average voltage $E(v_r) = 0.1112$.

5.2. Performances quantification with respect to noise acceleration excitation strength

To test the effectiveness of the proposed theoretical method on different noise intensities, a wide range of excitation acceleration strength $0<2D\leq0.5$ is adopted in this study. The theoretical predictions of the rectified voltage, electric power, and probability of the oscillation state in the snap-through regime in accompany with numerical counterparts are displayed

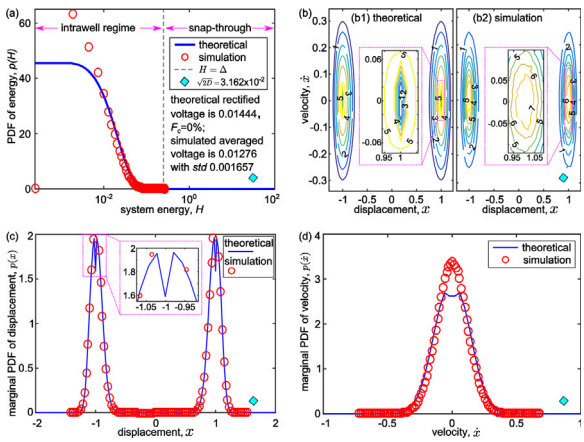

Fig. 3. Comparisons of theoretical predictions and numerical simulations on (a) probability density distribution of the system energy, (b) joint probability density of the displacement and velocity, (c) marginal probability density of the displacement, and (d) marginal probability density of the velocity of the harvester system driven by random acceleration excitation with intensity $\sqrt{2D} = 3.162\text{x}10^{-2}$ by which the dominant vibration states of the bistable harvester are in the intrawell regime.

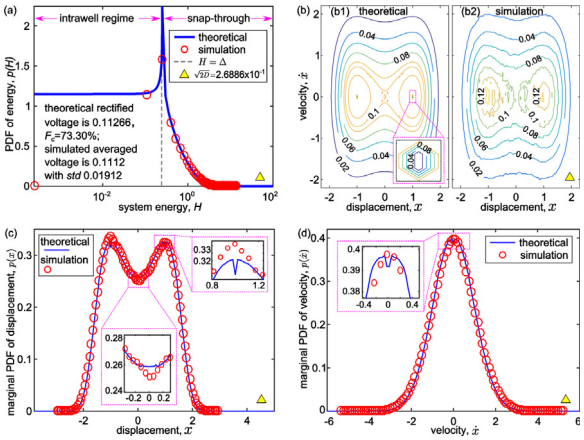

Fig. 4. Study case with the white noise excitation acceleration intensity $\sqrt{2D} = 2.6886 \times 10^{-1}$. Theoretical predictions and numerical simulations are compared on (a) probability density distribution of the system energy, (b) joint probability density of the displacement and velocity, (c) marginal probability density of the displacement, and (d) marginal probability density of the velocity.

in Fig. 5(a) and (b), and (c), respectively, in which the solid curves denote the theoretical results. For the numerical simulations as the circles shown in Fig. 5, those in (a) and (b) reveal the mean and standard deviation of the harvested voltage and power, and those in (c) are statistical probabilities of the energies in the range $H > \Delta$ counting from the 10^8-sample-long instantaneous system energies which are pre-evaluated via Eq. (13) in which the relation of N_H and H is approximated via theoretical predictions described in Section 3.2.

It is revealed that the harvested power almost increases proportionally with the base acceleration strength, which is corroborated from Fig. 5(a) in which the acceleration strength governs the rectified voltage in a quadric manner. From the insets in Fig. 5(c), the notable $p(H)$ spans a wider range in the area $H > \Delta$ under larger acceleration strength than that under weaker strength, resulting to the gradually increased F_c which trends to finally stabilize at as close to 1. Although the application of the stochastic averaging in principle confines to weak acceleration excitation [55], the theoretical results predicted through stochastic averaging approach still possesses high precision even for relatively strong excitation acceleration intensity.

5.3. *Effects of system parameters*

The dependence of the harvester performance on system parameters, including damping constant γ, time constant λ, and coupling coefficient Θ, are theoretically investigated and numerically validated here. Without special declaration hereafter, the unmentioned system parameters are the same as those listed in Table 2. Adopting the noise strength of $2D = 0.1$, Fig. 6(a) and (b) depict the rectified voltage and harvested power in a wide range of damping constant $10^{-5} \le \gamma \le 10^{-1}$, respectively. Both the harvested voltage and power monotonously decrease with increment of the damping constant, in consistent with the gradually decreased F_c calculated from both theoretical and simulation methods. Moreover, the theoretical predictions of the voltage and power are in good agreement with simulation results, exhibiting good robustness of the theoretical method under different damping constants.

Fig. 7(a) and (b) show the dependence of the rectified voltage and harvested electric power on a wide range of scaled time constant $6.468 \times 10^{-2} \le \lambda \le 6.468 \times 10^{3}$ with the base acceleration strength fixed at $2D = 0.12$. Based on the non-dimensional transformation formula in Eq. (2b) as well as an assumption that only the load resistance R varies with λ, the

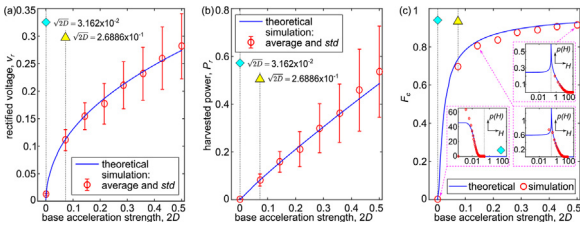

Fig. 5. Noise acceleration strength dependent (a) harvested rectified voltage, (b) extracted electric power, and (c) statistical proportion of oscillating states in the snap-through regime. The diamond and triangle symbols denote the corresponding example cases in Fig. 3, and Fig. 4, respectively. The inserts in (c) show the probability densities of the system energy when different excitation acceleration strengths drive the bistable harvester.

influence of the resistive load on the harvested voltage and power are captured and displayed in Fig. 7(c) and (d), respectively. Considering that the charging time for the electrical circuit getting into stationary state turns to be large for relatively low λ, a much longer simulation duration that producing 2.25×10^8-sample-long displacements and velocities are numerically estimated, of which their mean values and standard deviations are further evaluated and shown via circles in Fig. 7. Recalling the inverse proportional relation of the scaled time constant and load resistance, λ and R exhibit inverse effects on the system performance. With increment of the load resistance, the rectified voltage $\overline{v}_r$ increases while its increment rate increases initially and decreases afterwards, resulting to the convex-curve like harvested power $\overline{P}_r$. Additionally, it is apparent that the theoretical predictions by the proposed method accurately track the simulation counterparts and also effectively predict the optimal parameters that inducing the highest extracted power.

From Fig. 7, it also reveals that the standard deviation of the rectified voltage in simulation is in positive correlation with the mean value of the rectified voltage. The pentagon symbols in Fig. 7(a) denote the ratio of the standard deviation to the mean value of the rectified voltages, and it shows that the ratio decreases initially and increases afterwards with increment of the parameter λ. To explain that phenomena, the probability of the stochastic vibrations being in the snap-through state, F_c, is estimated from the simulated vibrations and denoted via triangle symbols in Fig. 7(b), and the trajectories of the simulated rectified voltages under three different parameters λ are shown in Fig. 8. The harvester oscillations contain random vibrations in single state and states switching. From Fig. 7(b), snap-through vibration is the primary vibration form while F_c decreases with decrement of λ, meaning that the states switching becomes frequently and thus the standard deviation becomes large. Meanwhile, considering that the mean value of the rectified voltage increases while its increment rate increases initially and decreases afterwards with decrement of λ, the ratio of the standard derivation to the mean value decreases initially and increases afterwards with decrement of λ in Fig. 7(a).

To investigate the influence of the non-dimensional coupling constant Θ on harvester performance and test the prediction effectiveness of the proposed method, the rectified voltage and the harvested electric power are evaluated on a wide range of non-dimensional coupling Θ varying from 3.337×10^{-8} to 3.337 with the white noise density chosen as $2D = 0.09$, and are shown in Fig. 9(a) and (b), respectively.

Fig. 9 reveals that the DC voltage and power keep near constant when Θ is relatively small such as less than Θ_1, while decreases with increment of Θ afterwards. It is also found that the proposed method could track the trend of the harvested voltage and power. For mild non-dimensional coupling constant such as less than and around Θ_1, the theoretical predictions exhibit good agreement with numerical simulations. While for relatively large coupling constants such as around and larger than Θ_2, the theoretically predicted voltage and power are finitely higher than those from simulations and their deviation turns to be larger with increment of Θ. To illustrate the causes of this estimation error, a mild coupling constant Θ_1 corresponding to the experiment setup, in contrast with a relatively large coupling constant Θ_2, are adopted for analysis and depicted using diamond and triangle symbols in Fig. 9, respectively. The J_H resulted from Θ_1 and Θ_2, denoting the damping effect of piezoelectric patch on harvester dynamics, are compared with the viscous damping constant γ in Fig. 9(c). It is observed that the J_H from mild coupling Θ_1 is several-magnitude less than γ, while that resulted from Θ_2 is two-order magnitude higher than γ which conflicts with the precondition of stochastic averaging method. Though the trade off in

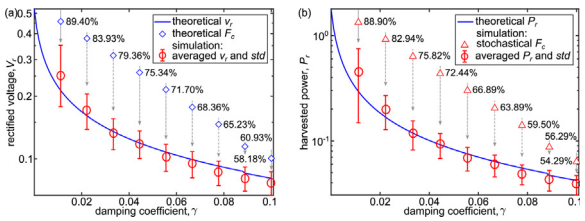

Fig. 6. The dependence of (a) the rectified voltage and (b) harvested electric power on the viscous damping coefficient γ with $2D = 0.1$. The diamond and triangle symbols denote the theoretically predicted state probability of the harvester in the snap-through regime F_c under each damping coefficient, and the statistically evaluated counterparts from simulated responses, respectively.

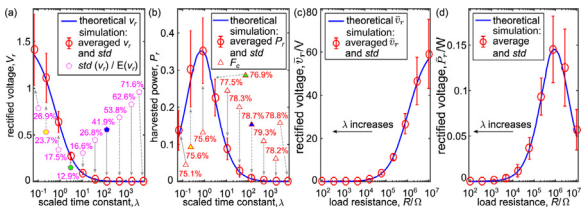

Fig. 7. The dependence of non-dimensional (a) rectified voltage and (b) harvested power on the scaled time constant λ with the base acceleration strength fixed at $2D = 0.12$, and the influences of the load resistance R on (c) the rectified voltage and (d) harvested power across R evaluated from (a) and (b) when only R varies with λ.

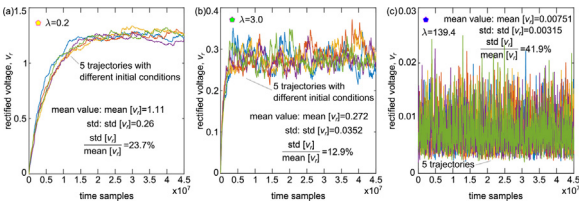

Fig. 8. Trajectories of the rectified voltage simulated via the Milstein method, and the filled pentagon symbols indicate the cases with different parameter λ in Fig. 7: (a) $\lambda = 0.2$, (b) $\lambda = 3.0$ and (c) $\lambda = 139.4$.

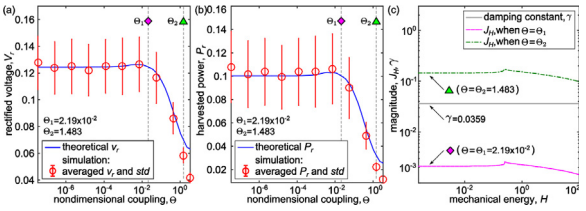

Fig. 9. The dependence of non-dimensional (a) rectified voltage and (b) harvested electric power on the non-dimensional coupling constant Θ with the base acceleration strength chosen as $2D = 0.09$. The diamond symbol denotes a mild Θ_1 that is evaluated from the experimental structure, while the triangle symbol denotes a large Θ_2 around and larger than which obvious deviation is presented between the theoretical prediction and stochastic simulation. (c) The corresponding J_H of Θ_1 and Θ_2 with respect to the mechanical energy H.

prediction for relatively large coupling constant, the theoretical predictions correctly track the performance trend and are in good agreement with numerical counterparts in a wide range of coupling constant.

6. Experimental investigation

To test the effectiveness of the developed theoretical approach, the energy conversion predictions are validated through experiments conducted on the system described in Fig. 2 across a wide range of random acceleration strengths. Random vibrations of the shaker with the frequency spectrum span in the range [0, 90Hz] are generated with tunable statistical variance controlled via the gain of the shaker. The base acceleration is measured via the accelerometer with the sampling frequency of 2048Hz, and the instantaneous acceleration signals are shown in Fig. 10. From Fig. 10(a), it is calculated that the standard deviation of the base acceleration is 2.5027ms^{-2}. According to the formulas that Erturk and Inman derived in the equivalent lumped element model from the realistic, continuous beam system [56], a correction factor is taken into account to multiply the base acceleration density by 1.566, which results to the effective noise acceleration strength of $\sqrt{D_0} = 3.9192\text{ms}^{-2}$ in the case.

To test the system performance under different excitation acceleration strengths, the gain of the shaker is chosen from a linearly spaced range of 6 values over its whole tunable range, such that to generate 6 standard deviations of the base acceleration. The effective noise acceleration strengths $\sqrt{D_0}$ are measured to be 1.4697m/s^2, 3.9192m/s^2, 5.7814m/s^2, 7.7254m/s^2, 10.9186m/s^2, and 15.3084m/s^2, respectively. Under each acceleration level, two kinds of filter capacitances, $C_r = 47\mu$F and $C_r = 470\mu$F, are individually and successively connected in the standard rectifying electrical circuit. The base motion for each noise acceleration strength and filter capacitance is set to last for 40min, ensuring that the charging system reaches statistically stationary and sufficient data are obtained for statistical estimation. After the data are recorded, the expectation value of the rectified voltage is calculated as the sum of the averaged voltage across the load resistance and voltage drop across the diodes during the stationary interval of the harvester motion from 120s to 2400s. The mean harvested power is further evaluated from the instantaneous electric power $P_r = v_r^2/R$ during the same time interval for stationary vibrations. Fig. 11(a) and (b), separately displays the experimentally measured mean rectified voltages and harvested electric

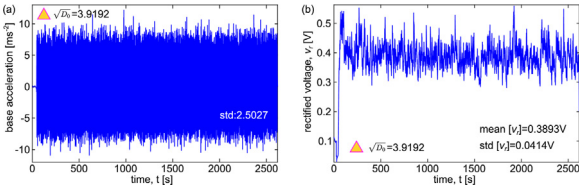

Fig. 10. Experimentally measured instantaneous (a) base acceleration and (b) rectified voltages. The triangle symbol denotes the noise acceleration strength of $\sqrt{D_0} = 3.9192\text{ms}^{-2}$.

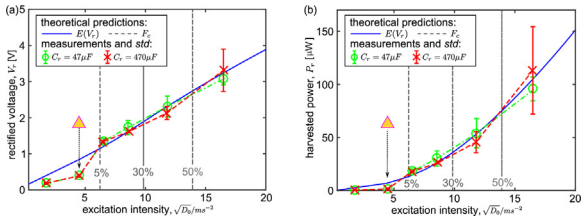

Fig. 11. Experimentally measured (a) rectified voltage and (b) harvested power of the bistable harvester interfaced with the standard rectifying electrical circuit driven by different-intensity white noise excitation accelerations.

powers accompanied with their statistical standard deviations from the interfaced system under different white noise acceleration intensities, as well as the theoretically predicted counterparts from the developed stochastic averaging method.

The dashed (gray) lines in Fig. 11 locate the acceleration intensities where the theoretical predictions of the statistical snap-through state probability F_c are 5%, 30% and 50%, respectively, indicating that the noise acceleration intensities span a relatively wide range from non-dominant case of the statistical snap-through state with $F_c < 5\%$ to the completely dominant case of the statistical snap-through state with $F_c > 50\%$. Also, both experimental measurements and theoretical predictions indicate that the harvested rectified voltage and electric power, as well as the statistical state proportion in snap-through regime increase with increment of the acceleration excitation strength. Comparing the theoretical predictions with experimental measurements, it reveals that their trends are in good agreement in the wide range of white noise acceleration intensities. While obvious deviations are observed when the base acceleration intensity is relatively weak, which could be explained by the difference of experimental and theoretical models when the voltage drop across the diodes is significant compared with that across the load resistance. Additionally, the mean measurements from the two different filter capacitances are found to be close to each other, while the standard deviation of measurements from larger filter capacitance $C_r = 470\mu$F remains smaller than that from smaller capacitance $C_r = 47\mu$F under each base acceleration level, excepting for only one experiment case of the highest excitation acceleration level, validating that relatively large filter capacitance is expected to obtain near-constant harvested voltage and power for electronics in engineering applications.

7. Conclusion

To extract DC voltage from environment-like, random vibrations, a nonlinear electromechanical coupling system of a bistable energy harvester interfaced with a standard rectifying electrical circuit is considered in this research. A theoretical method is established to predict the stationary statistic dynamics and electrical energy harvesting performance of the interfaced system when driven by white noise accelerations, and numerical and experimental efforts are employed to validate the theoretically derived insights. Two representative examples exhibit the effectiveness of the theoretical method on predicting the joint and marginal PDFs of the vibration variables, as well as the PDF of the system energy. Also, the probability of vibration state in snap-through or intrawell regimes is estimated via interval integration of the PDF of system energy, and is validated in good agreement with simulation counterpart under different base acceleration strengths. Moreover, the proposed approach provides an effective tool to identify the effects of acceleration strength and system design parameters on the energy harvesting performance. It is revealed that the noise acceleration excitation density governs the harvested electric power in a nearly linear manner, and the probability of snap-through vibration state increases dramatically in the range of moderate noise strength and remains almost constant around 0.9 for relatively large acceleration strength. The harvesting performance is also dependent on the system damping constant, load resistance, and electromechanical coupling, while their effects are different. The nondimensional rectified voltage and harvested power monotonically decrease with increment of the damping constant, while remain near constant for moderate nondimensional coupling and decrease dramatically for relatively large nondimensional coupling constant. Thus, there exists the optimal coupling constant and load resistance to enlarge the harvested power, which could be evaluated via the proposed theoretical method. Additionally, despite the trade off in predictive ability under relatively large nondimensional coupling, the proposed method is validated to provide good predictions of the energy harvesting performance as compared with the numerical and experimental results.

Acknowledgments

This work is supported in part by the National Natural Science Foundation of China (No. 51475356), China Postdoctoral Science Foundation grant 2018M631196, the University of Michigan Collegiate Professorship, and the U.S. National Science Foundation grants 1661572 and 1661568.

References

[1] Y.-J. Hu, I.-C. Chen, T.-H. Tsai, A piezoelectric vibration energy harvesting system with improved power extraction capability, in: IEEE Asian Solid-state Circuits Conference, Toyama, Japan, November 7-9, 2016.
[2] S. Priya, D.J. Inman, Energy Harvesting Technologies, Springer, New York, 2009.

[3] S. Leadenham, A. Erturk, M-shaped asymmetric nonlinear oscillator for broadband vibration energy harvesting: harmonic balance analysis and experimental validation, J. Sound Vib. 333 (2014) 6209–6223.
[4] H. Xue, Y. Hu, Q. Wang, Broadband piezoelectric energy harvesting devices using multiple bimorphs with different operating frequencies, IEEE Trans. Ultrason. Ferroelectrics Freq. Contr. 55 (2008) 2104–2108.
[5] P. Kim, J. Seok, A multi-stable energy harvester: dynamic modeling and bifurcation analysis, J. Sound Vib. 333 (2014) 5525–5547.
[6] J. Cao, S. Zhou, W. Wang, J. Lin, Influence of potential well depth on nonlinear tristable energy harvesting, Appl. Phys. Lett. 106 (2015) 173903.
[7] H. Fang, S. Li, H. Ji, K. Wang, Dynamics of a bistable miura-origami structure, Phys. Rev. 95 (5) (2017) 052211.
[8] W.-A. Jiang, L.-Q. Chen, Snap-through piezoelectric energy harvesting, J. Sound Vib. 333 (2014) 4314–4325.
[9] R. Harne, K. Wang, A review of the recent research on vibration energy harvesting via bistable systems, Smart Mater. Struct. 22 (2013) 023001.
[10] S.P. Pellegrini, N. Tolou, M. Schenk, J.L. Herder, Bistable vibration energy harvesters: a review, J. Intell. Mater. Syst. Struct. 24 (11) (2012) 1303–1312.
[11] R. Harne, K. Wang, Harnessing Bistable Structural Dynamics: for Vibration Control, Energy Harvesting, and Sensing, John Wiley and Sons, 2017.
[12] R. Harne, M. Thota, K. Wang, Concise and high-fidelity predictive criteria for maximizing performance and robustness of bistable energy harvesters, Appl. Phys. Lett. 102 (2013) 053903.
[13] S.R. Panigrahi, B.F. Feeny, A.R. Diaz, Harmonic balance analysis of snap-through orbits in an undamped Duffing oscillator, J. Vib. Acoust. 137 (6) (2015) 064502.
[14] W. Liu, A. Badel, F. Formosa, Y. Wu, A. Agbossou, Novel piezoelectric bistable oscillator architecture for wideband vibration energy harvesting, Smart Mater. Struct. 22 (2013) 035013.
[15] S.C. Stanton, C.C. McGehee, B.P. Mann, Nonlinear dynamics for broadband energy harvesting: investigation of a bistable piezoelectric inertial generator, Physica D 239 (2010) 640–653.
[16] C. Lan, W. Qin, Enhancing ability of harvesting energy from random vibration by decreasing the potential barrier of bistable harvester, Mech. Syst. Signal Process. 85 (2017) 71–81.
[17] H. Wang, L. Tang, Modeling and experiment of bistable two-degree-of-freedom energy harvester with magnetic coupling, Mech. Syst. Signal Process. 86 (2017) 29–39.
[18] R. Harne, C. Zhang, B. Li, K. Wang, An analytical approach for predicting the energy capture and conversion by impulsively-excited bistable vibration energy harvesters, J. Sound Vib. 373 (2016) 205–222.
[19] C. Zhang, R. Harne, B. Li, K. Wang, Reconstructing the transient,dissipative dynamics of a bistable DUffing oscillator with an enhanced averaging method and Jacobian elliptic functions, Int. J. Non Lin. Mech. 79 (2016) 26–37.
[20] Q. Dai, R. Harne, Investigation of direct current power delivery from nonlinear vibration energy harvesters under combined harmonic and stochastic excitations, J. Intell. Mater. Syst. Struct. (2017), https://doi.org/10.1177/1045389X17711788.
[21] P. Kumar, S. Narayanan, S. Adhikari, M. Friswell, Fokker-Planck equation analysis of randomly excited nonlinear energy harvester, J. Sound Vib. 333 (2014) 2040–2053.
[22] Q. He, M.F. Daqaq, New insights into utilizing bistability for energy harvesting under white noise, J. Vib. Acoust. 137 (2015) 021009.
[23] G. Litak, M. Friswell, S. Adhikari, Magnetopiezo elastic energy harvesting driven by random excitation, Appl. Phys. Lett. 96 (2010) 214103.
[24] G. Litak, M. Borowiec, M.I. Friswell, S. Adhikarl, Energy harvesting in a magnetopiezoelastic system driven by random excitations with uniform and Gaussian distributions, J. Theor. Appl. Mech. 49 (3) (2011) 757–764.
[25] R. Masana, M.F. Daqaq, Response of duffing-type harvesters to band-limited noise, J. Sound Vib. 332 (2013) 6755–6767.
[26] Q. He, M.F. Daqaq, Influence of potential function asymmetries on the performance of nonlinear energy harvesters under white noise, J. Sound Vib. 333 (2014) 3479–3489.
[27] A.S.D. Paula, D.J. Inman, M.A. Savi, Energy harvesting in a nonlinear piezomagneto elastic beam subjected to random excitation, Mech. Syst. Signal Process. 54–55 (2015) 405–416.
[28] S. Zhao, A. Erturk, On the stochastic excitation of monostable and bistable electroelastic power generators: relative advantages and tradeoffs in a physical system, Appl. Phys. Lett. 102 (2013) 103902.
[29] D.J. Tweten, B.P. Mann, Experimental investigation of colored noise in stochastic resonance of a bistable beam, Physica D 268 (2014) 25–33.
[30] W. Martens, U. v. Wagner, G. Litak, Stationary response of nonlinear magnetopiezoelectric energy harvester systems under stochastic excitation, Eur. Phys. J. Spec. Top. 222 (2013) 1665–1673.
[31] D. Meimukhin, N. Cohen, I. Bucher, On the advantage of a bistable energy harvesting oscillator under band-limited stochastic excitation, J. Intell. Mater. Syst. Struct. 24 (14) (2013) 1736–1746.
[32] M.F. Daqaq, Transduction of a bistable inductive generator driven by white and exponentially correlated Gaussian noise, J. Sound Vib. 330 (2011) 2554–2564.
[33] P. Green, K. Worden, N. Sims, On the identification and modeling of friction in a randomly excited energy harvester, J. Sound Vib. 332 (2013) 4696–4708.
[34] R. Harne, K. Wang, Prospects for nonlinear energy harvesting systems designed near the elastic stability limit when driven by colored noise, J. Vib. Acoust. 136 (2014) 021009.
[35] G.K. Ottman, H.F. Hofmann, A.C. Bhatt, G.A. Lesieutre, Adaptive piezoelectric energy harvesting circuit for wireless remote power supply, IEEE Trans. Power Electron. 17 (2002) 669–676.
[36] Y. Shu, I. Lien, Analysis of power output for piezoelectric energy harvesting systems, Smart Mater. Struct. 15 (2006) 1499–1512.
[37] J. Liang, W.-H. Liao, Improved design and analysis of selt-powerd synchronized switch interface circuit for piezoelectric energy harvesting systems, IEEE Trans. Ind. Electron. 59 (2012) 1950–1960.
[38] E. Lefeuvre, A. Badel, C. Richard, Energy harvesting using piezoelectric materials: case of random vibrations, J. Electroceram. 19 (2007) 349–355.
[39] Y.-Y. Chen, D. Vasic, Y.-P. Liu, F. Costa, Study of a piezoelectric switching circuit for energy harvesting with bistable broadband technique by work-cycle analysis, Intell. Mater. Syst. Struct. (2012), 1045389X12460339.
[40] W. Liu, A. Badel, F. Formosa, Y. Wu, A. Agbossou, Wideband energy harvesting using a combination of an optimized synchronous electric charge extraction circuit and a bistbale harvester, Smart Mater. Struct. 22 (2013) 125038.
[41] K.A. Singh, R. Kumar, R.J. Weber, A broadband bistbale piezoelectric energy harvester with nonlinear high-power extraction, IEEE Trans. Power Electron. 30 (12) (2015) 6763–6774.
[42] F. Cottone, L. Gammaitoni, H. Vocca, M. Ferrari, V. Ferrari, Piezoelectric buckled beams for random vibration energy harvesting, Smart Mater. Struct. 21 (2012) 035021.
[43] F. Dinca, C. Teodosiu, Nonlinear and Random Vibration, Academic, 1973.
[44] W. Zhu and Y. Lin, "Stochastic Averaging of Energy Envelope," vol. **117** (8), pp. 1890-1905, 1991.
[45] Y. Lin, G. Cai, Probabilistic Structural Dynamics: Advanced Theory and Application, McGraw-Hill, 1995.
[46] J. Liang, W.-H. Liao, Impedance modeling and analysis for piezoelectric energy harvesting systems, IEEE ASME Trans. Mechatron. 17 (6) (2012) 1145–1157.
[47] P. Byrd, M. Friedmand, Handbook of Elliptic Integrals for Engineers and Physicists, Springer-Verlag, Berlin, 1954.
[48] C. Gardiner, Handbook of Stochastic Method, Springer, Berlin, 1985.
[49] R. Khasminskii, Stochastic Stability of Differential Equations, Springer Science & Business Media, 2011.
[50] R. Wiebe, L. Virgin, On snap-through buckling, in: 52nd AIAA/ASME/ASCE/AHS/ASC Structures, Structural Dynamics and Materials Conference, Denver, Colorado, April 4–7, 2011.
[51] R. Stratonovitch, Topics in the Theory of Random Noise, Gordon and Breach, New York, 1963.
[52] S.S. Rao, F.F. Yap, Mechanical Vibration, fourth ed., Addison-Wesley, 1995.

[53] U. Picchini. [Online]. Available: http://sdetoolbox.sourceforge.net.
[54] Z. Botev. [Online]. Available: https://www.mathworks.com/matlabcentral/fileexchange/17204-kernel-density-estimation.
[55] M. Xu, X. Jin, Y. Wang, Z. Huang, Stochastic averaging for nonlinear vibration energy harvesting system, Nonlinear Dynam. 78 (2014) 1451–1459.
[56] A. Erturk, D. Inman, Issues in mathematical modeling of piezoelectric energy harvesters, Smart Mater. Struct. 3 (2008) 041001.